12-29-2006

A New View of Ridge Segmentation and Near-Axis Volcanism at the East Pacific Rise, 8°–12°N, from EM300 Multibeam Bathymetry

Scott M. White
University of South Carolina - Columbia, swhite@geol.sc.edu

Rachel M. Haymon
University of California - Santa Barbara

S M. Carbotte
Columbia University

Publication Info

Published in *Geochemistry, Geophysics, Geosystems*, Volume 7, Issue 12, 2006, pages 1-12.

Geochemistry Geophysics Geosystems G3
AN ELECTRONIC JOURNAL OF THE EARTH SCIENCES
Published by AGU and the Geochemical Society

Data Brief
Volume 7, Number 12
29 December 2006
Q12O05, doi:10.1029/2006GC001407
ISSN: 1525-2027

A new view of ridge segmentation and near-axis volcanism at the East Pacific Rise, 8°–12°N, from EM300 multibeam bathymetry

Scott M. White
Department of Geological Sciences, University of South Carolina, 701 Sumter Street, Columbia, South Carolina 29208, USA (swhite@geol.sc.edu)

Rachel M. Haymon
Department of Earth Sciences, University of California, Santa Barbara, Santa Barbara, California 93106, USA

Suzanne Carbotte
Lamont-Doherty Earth Observatory, Columbia University, Palisades, New York 10964, USA

[1] New, high-resolution bathymetry for the East Pacific Rise between 8°N and 12°N was collected over a 6 km wide swath centered on the ridge axis using the 30 kHz Simrad EM300 multibeam system. The coverage area corresponds latitudinally to the designated Ridge2000 Integrated Studies Site (ISS) for fast spreading ridges. The EM300 data, gridded at 30 m latitude by 50 m longitude, represent a greater than 4X improvement in horizontal resolution over previously available multibeam data and a 2X improvement in depth resolution. The new bathymetry was used to update the locations and hierarchy of ridge offsets for this area. Among the many applications for this data, it enables us to tabulate volcanoes half the size that could be previously detected. The distribution of near-axis volcanic cones >25 m high suggests that this population of small, near-axis cones results from low effusion rate eruptions of the ridge axis.

Components: 4480 words, 5 figures, 1 table, 1 animation.

Keywords: bathymetry; seafloor spreading; seamounts; segmentation.

Index Terms: 3035 Marine Geology and Geophysics: Midocean ridge processes; 3045 Marine Geology and Geophysics: Seafloor morphology, geology, and geophysics; 3075 Marine Geology and Geophysics: Submarine tectonics and volcanism.

Received 30 June 2006; **Revised** 4 October 2006; **Accepted** 18 October 2006; **Published** 29 December 2006.

White, S. M., R. M. Haymon, and S. Carbotte (2006), A new view of ridge segmentation and near-axis volcanism at the East Pacific Rise, 8°–12°N, from EM300 multibeam bathymetry, *Geochem. Geophys. Geosyst.*, *7*, Q12O05, doi:10.1029/2006GC001407.

Theme: Formation and Evolution of Oceanic Crust Formed at Fast Spreading Rates
Guest Editors: Damon A. H. Teagle and Doug Wilson

1. Introduction

[2] The East Pacific Rise (EPR) between 8°N and 12°N is an area of intense investigation into the process of seafloor spreading, and was recently designated the type area for fast spreading rates by the Ridge 2000 Program (Figure 1). The advent of multibeam mapping systems in the early 1980s provided the first continuous coverage maps of the rise crest throughout this area [*Macdonald et al.*, 1984]. The most comprehensive map for this area has ~300 m grid cell size from transit satellite navigated SeaMARC II phase bathymetry [*Macdonald et al.*, 1992]. SeaBeam coverage of the axis gridded at 100 m is available but is based on transit satellite navigation [*Tighe et al.*, 1988]. Poor navigation from transit satellite and dithered GPS limited the resolution of these gridded data sets. Since then, progress on multibeam mapping has been made, but the areas mapped have been much more limited in extent (Figure 1). Smaller areas mapped by SeaBeam with P-code GPS navigation have been gridded at 80 m [*Cochran et al.*, 1999; *Wilcock et al.*, 1993]. The Simrad EM300 multibeam system represents a fundamental advance over previous systems in that it uses 30 kHz sound and 1° × 1° beam width, rather than 12 kHz and 2° or 2.67° beams, to ensonify the seafloor. The main purpose of this paper is to present a digital map series from the first EM300 survey of the EPR collected during 2005 aboard the R/V *Thompson*.

[3] The EM300 bathymetry represents an important advance over the previously available maps and bathymetric data. It is both high-resolution and spatially extensive, covering the entire length of ridge within the EPR Ridge 2000 Integrated Studies Site. Perhaps the most significant is that it is well navigated from continuous, undithered, differential GPS that has only been available since 1991. The new higher-resolution EM300 multibeam data set allows us to reexamine with the benefit of bathymetric data the small axial discontinuities picked previously from side-scan acoustic backscatter images. The new EM300 maps also can be used to examine detailed structure on the crest of the EPR at a scale that bridges the gap between local, highly detailed near-bottom mapping and regional, lower-resolution surface vessel sonar mapping. Two highlights that we comment on in this work are the hierarchy of ridge discontinuities and the distribution of small (>25 m high) near-axis volcanic cones.

2. Data Acquisition

[4] The Simrad EM300 multibeam sonar system on the R/V *Thompson* collected a single swath of bathymetry along the ridge crest of the EPR from 8°N to 12°N in November 2005 during a transit leg between San Diego, USA and Puerto Ayora, Galápagos. The entire survey was navigated using the C-Nav™ GcGPS, a real-time differential correction with submeter accuracy. The low horizontal dilution of precision, the stable series of position fixes, and a very favorable comparison between the new EM300 data and the transponder-net navigated ABE bathymetry from the EPR (V. Ferrini, personal communication, 2006) all suggest that navigation was excellent throughout the survey. The data were transmitted from ship to shore using HiSeasNet [*Berger et al.*, 2006] during the survey, and was shown in preliminary form at the fall 2005 American Geophysical Union meeting while the cruise was still underway.

[5] The EM300 system operates at 30 kHz. This frequency allows for 5 m vertical resolution and smaller beam footprints compared to the standard 10–15 kHz multibeam systems aboard most research vessels. The EM300 system is a highly adaptable system, and uses active beam steering for control of the beam spacing to help maintain an even swath width and full bottom coverage. The positions of the beams were corrected for the ship's pitch, roll, heave, and yaw by a POS M/V inertial reference system. The sea state was fairly low during the survey, and despite having a headwind that caused the heading to deviate consistently from the course made good by ~5° to the east, little beam steering was necessary. The average pitch was bow-down 0.2° ± 0.5° with a maximum angle of 2.3°. The average roll was 1.3° ± 0.7° to port with a maximum roll angle of 4.7° during the survey.

[6] The EM300 installed on the R/V *Thompson* transmits 135 beams per ping over a 120° angular swath using a steered beamforming array. The swath was ~6 km during the survey, yielding an expected across-track beam spacing of ~45 m. The EM300 uses both amplitude and phase detection to measure the received sound, thus the working across-track resolution is somewhere between the beam spacing and beam footprint. During data collection, the EM300 was operated in an equal-

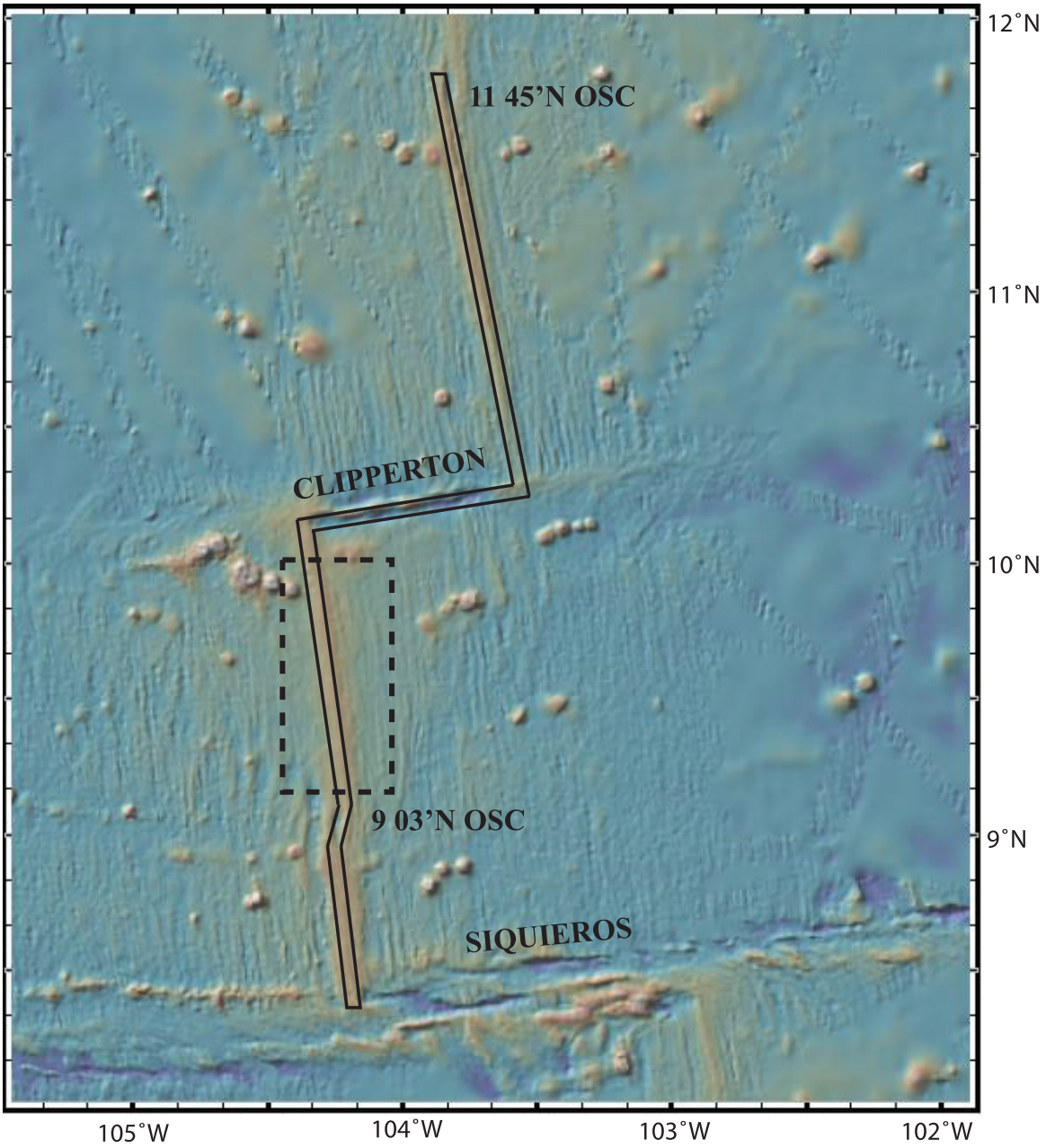

Figure 1. Overview of bathymetry from the study area, and its regional setting with respect to major ridge offsets (created by GeoMapApp, http://www.geomapapp.org). The shaded-relief areas of the map indicate where 300 m bathymetry grids from surface ship measurements are available; the remainder of the map is derived from satellite altimetry. The major, first- and second-order, ridge axis discontinuities are labeled. The solid line box shows the area of the EM300 sonar swath. The bold dashed lines outline the area where previous higher-resolution (80 m gridded) multibeam bathymetry is available.

area mode, where the beamformer projects beams of varying angle across the swath to create equal size sonar footprints on the seafloor. The ping rate is automatically adjusted by the sonar to the limit of the round-trip traveltime of sound in the water. The average ping rate during the survey was 7.0 ± 0.1 seconds s. The survey was run at 9–10 knots (4.6–5.1 ms^{-1}) speed over ground to maximize the survey area within time constraints imposed by the transit. Thus a 30–35 m along-track ping spacing is expected.

[7] The depth recorded by any echosounder is strongly dependent on the sound velocity profile through the water column. An expendable bathy-

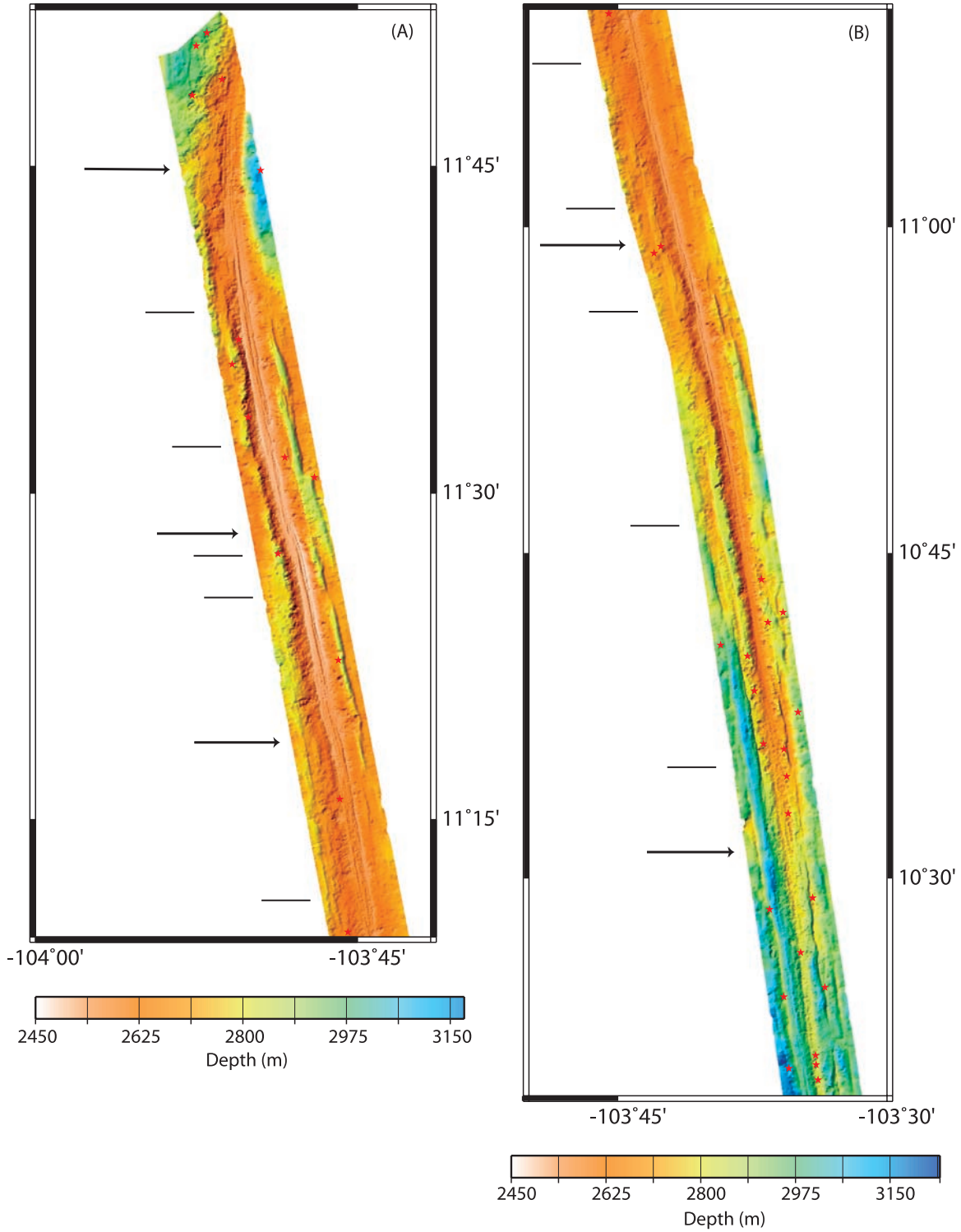

Figure 2. Shaded-relief bathymetric maps derived from 30 m × 50 m gridded EM300 depth measurements. Depth is plotted with a histogram-equalized color palette optimized for each panel to emphasize local changes in terrain. Locations of third-order (arrows) and fourth-order ridge discontinuities (lines) from Table 1 are indicated. Red stars indicate the location of each very-near-axis volcanic cone meeting the criteria explained in the text.

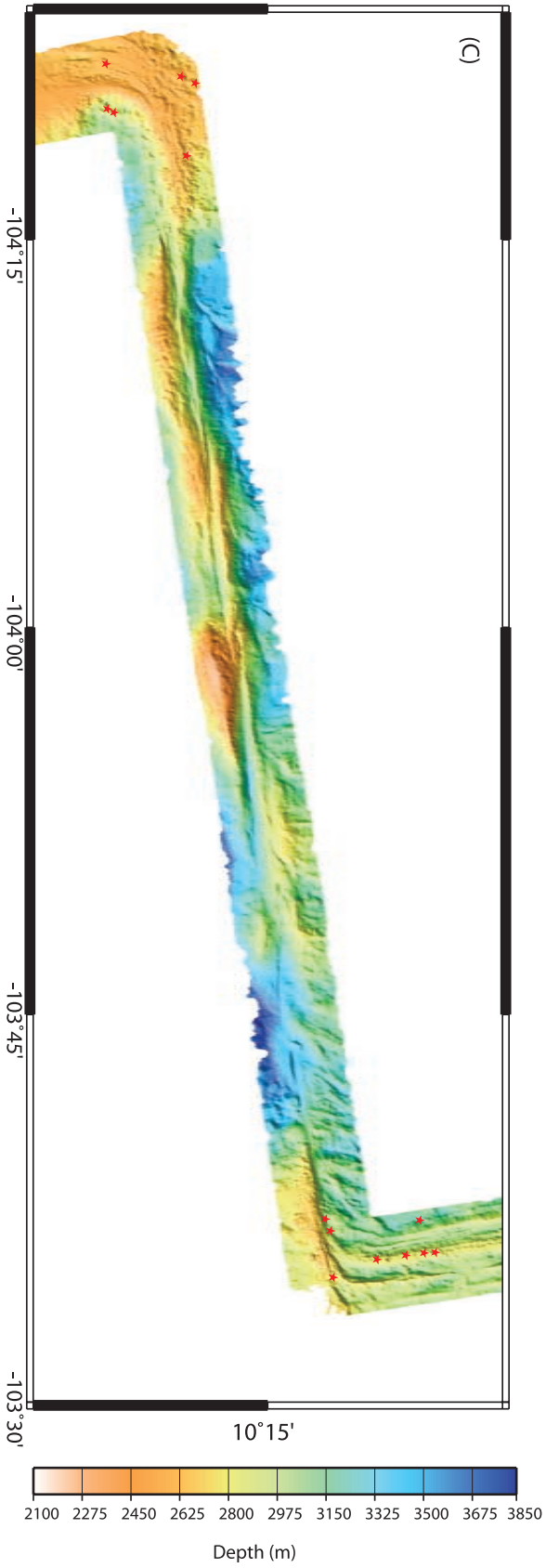

Figure 2. (continued)

thermograph (XBT) probe was used to obtain a sound velocity profile through the thermocline at the start of the survey. The sound velocity profile from this XBT was applied to all pings during the survey.

[8] The data were processed using the MB-system software [*Caress and Chayes*, 1996]. We found the bathymetric readings to be sufficiently noise-free so that no automatic filters were applied. Some manual editing of the individual pings reduced the noise near the edges of the swath. The majority of the swath remained >5.5 km wide after editing. A radial Gaussian basis function was applied to the points to search for the optimal grid spacing using the method described by *Ferrini et al.* [2007]. From this analysis, it was determined that density of data points supported gridding at 30 m (along-track, north-south) by 50 m (across-track, east-west). This corresponds to our estimates of along-track and across-track data resolution based on physical parameters. Higher resolution might have been obtained by setting the across-track width of the sonar swath to a maximum of 5 km. Gridding was done using the mbgrid module of MB-system in the weighted beam footprint mode, which assigns a depth value based on the fraction of the grid cell that the footprint of the beam covers. Interpolation was applied using a minimum curvature spline to fill gaps of 1 grid cell between two defined grid cells. An examination of the gridded data indicates that each gridcell contains an average of 1.25 data points. Grids were made for 12°N to the Clipperton Transform and from Clipperton south to the Siquieros Transform (Figure 2). These grids reside at the Ridge2000 data portal (http://www.marine-geo.org/link/entry.php?id=TN188).

3. Structure of the Ridge Crest

[9] Ridge discontinuities are particularly important because they divide the ridge into discrete units of crustal accretion. Between 8°N and 12°N, the EPR exhibits a full range of scales of ridge discontinuities, but smaller offsets north and south of the 9°–10°N segment are only roughly defined from transit-satellite navigated SeaMARC II side-scan data [see *Macdonald et al.*, 1992, Table 2]. These "fine-scale" offsets are subdivided into third or fourth order on the basis of criteria given by *Macdonald et al.* [1991] and *White et al.* [2000]. Although the resolution of the SeaMARC II side-scan data is similar to our EM300 bathymetry, improvements in navigational accuracy and the

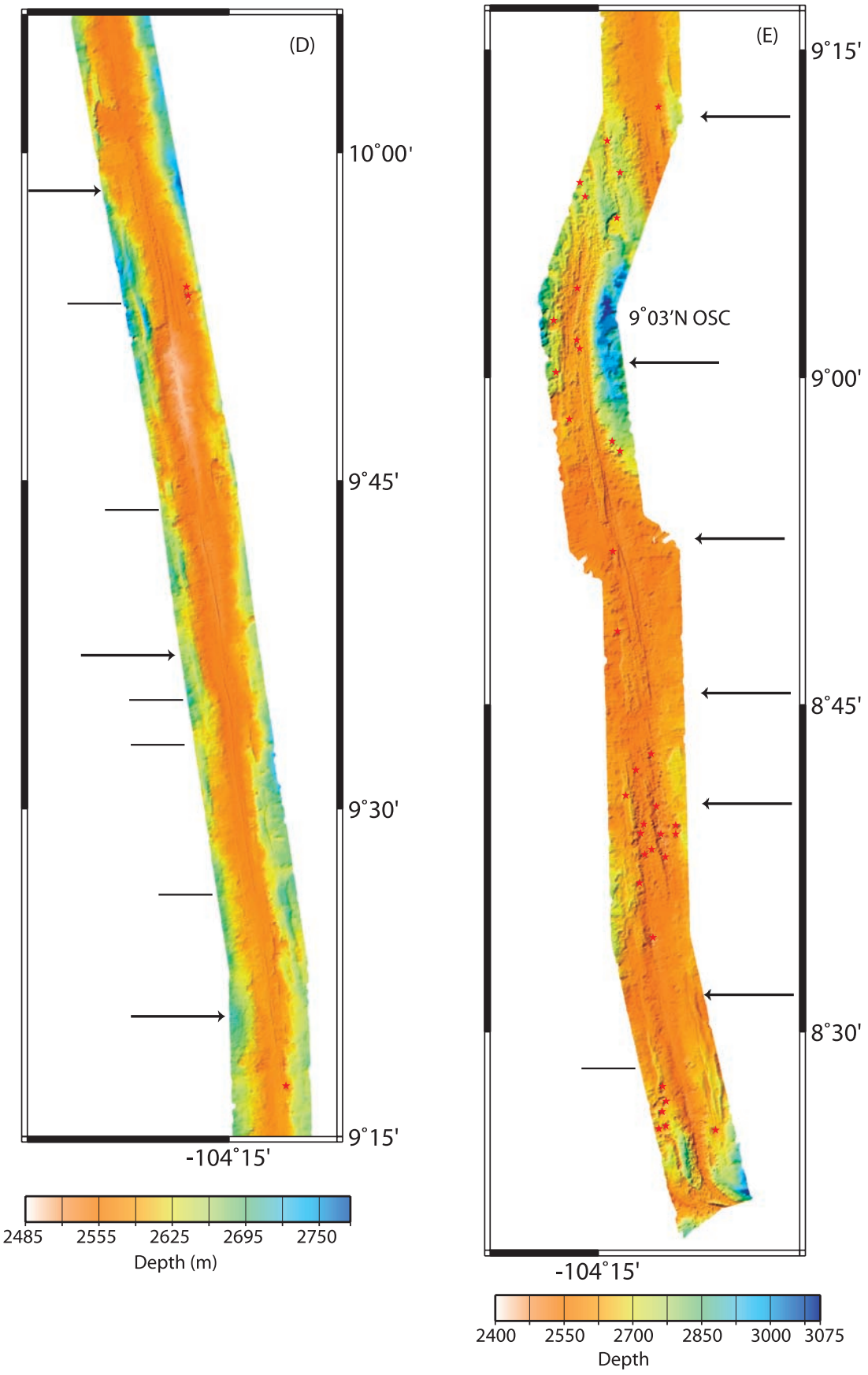

Figure 2. (continued)

Table 1. Location of Ridge Discontinuities on the EPR, 8°–12°N From EM300 Bathymetry[a]

Latitude, N	Order	Offset, km	Sense	Comment	See Also
8°24′	1	140	L	Siquieros	*Fornari et al.* [1989]
8°27.5′	4	0.1	R		
8°31′	3	0.5	R		
8°37′	3	2	R	overlapping ridges; overlap zone extends 8°36′–39′N G, M	
8°45.5′	3	0.4	R	transition from wide to narrow ASCT, discontinuity zone extends 8°45′–46′N M	
8°53′	3	0.5	L	S	
9°00.5′	3	1.5	L	end of ASCT	
9°03′	2	10	R	OSC G, M	*Kent et al.* [2000]; *Sempere and Macdonald* [1986]
9°12′	3	0.3	R		*Haymon et al.* [1991]; *White et al.* [2002]
9°20′	3	0.9	R	revised location from 9°17′N [*Haymon et al.*, 1991]; overlapping axial pillow ridges zone 9°21′–9°19′N G, S.	*White et al.* [2002]
9°26′	4	<0.1	-	M	*Haymon et al.* [1991]
9°32.7′	4	<0.1	R		*Haymon et al.* [1991]
9°34.9′	4	<0.1	R	bend in bathymetry	*Haymon et al.* [1991]
9°37′	3	0.5	R	overlapping ASCTs; overlap zone extends 9°36′–38′N M	*Smith et al.* [2001]; *Haymon et al.* [1991]
9°44′	3? Or 4	0.2	R	previously identified as third order [*White et al.*, 2002], but similar in total offset to other fourth order M	*Haymon et al.* [1991]
9°49′	4	0.1	R		*Haymon et al.* [1991]
9°53′	4	0.2	R	CCW rotation of ridge axis; could be 9°51.5′ RAD [*Haymon et al.*, 1991]? G	
9° 58′	3	>0.2	L	overlapping axial pillow ridges; overlap zone extends 9°55.7′–59′N M?	*White et al.* [2002]
10° 05′	4	<0.2	L	offset of small ASCT M	
10°15′	1	85	R	Clipperton	*Gallo et al.* [1986]; *Kastens et al.* [1986]
10°32′	3	0.7	R	G	at 10°31′ in *Macdonald et al.* [1992]
10°35.5′	4	0.2	R	poorly defined axial trace for 10°35′–36′N; several small offsets through this zone	
10°46.5′	4	0	-	CCW rotation of ridge axis	
10°56′	4	0.2	R	overlapping ASCTs; overlap zone extends 10°55.8′–56.3′N	
10°59′	3	0.3	R	offset in ASCT; seismic AMC reflector to present north, absent to south [*Detrick et al.*, 1987]	
11°01.5′	4	0.1	L	Offset in ASCT	
11°08′	4	0.2	R	G; S	
11°11′	4	0.2	R		
11°18.5′	3	0.3	R	at 11°19′ in *Langmuir et al.* [1986] G, M	
11°20.5′	4	0	-	CW rotation of ridge axis and minor offset in ASCT	
11°25′	4	<0.1	L	offset in ASCT	
11°28.5′	3	0.3	L	offset in ASCT G; S	
11°32′N	4	<0.1	L	axis shifts left from narrow to broad ASCT	
11°38′	4	0.2	R		
11°45′	2	9	R	OSC G, M, S	*Perram and Macdonald* [1990]

[a] Segmentation order defined by *White et al.* [2002], revised from *Macdonald et al.* [1991]. G, geochemical Deval from *Langmuir et al.* [1986]; M, magnetization anomaly from *Carbotte and Macdonald* [1992], *Perram and Macdonald* [1990], or *Lee et al.* [1996]; S, gap in seismic AMC reflector [*Detrick et al.*, 1987].

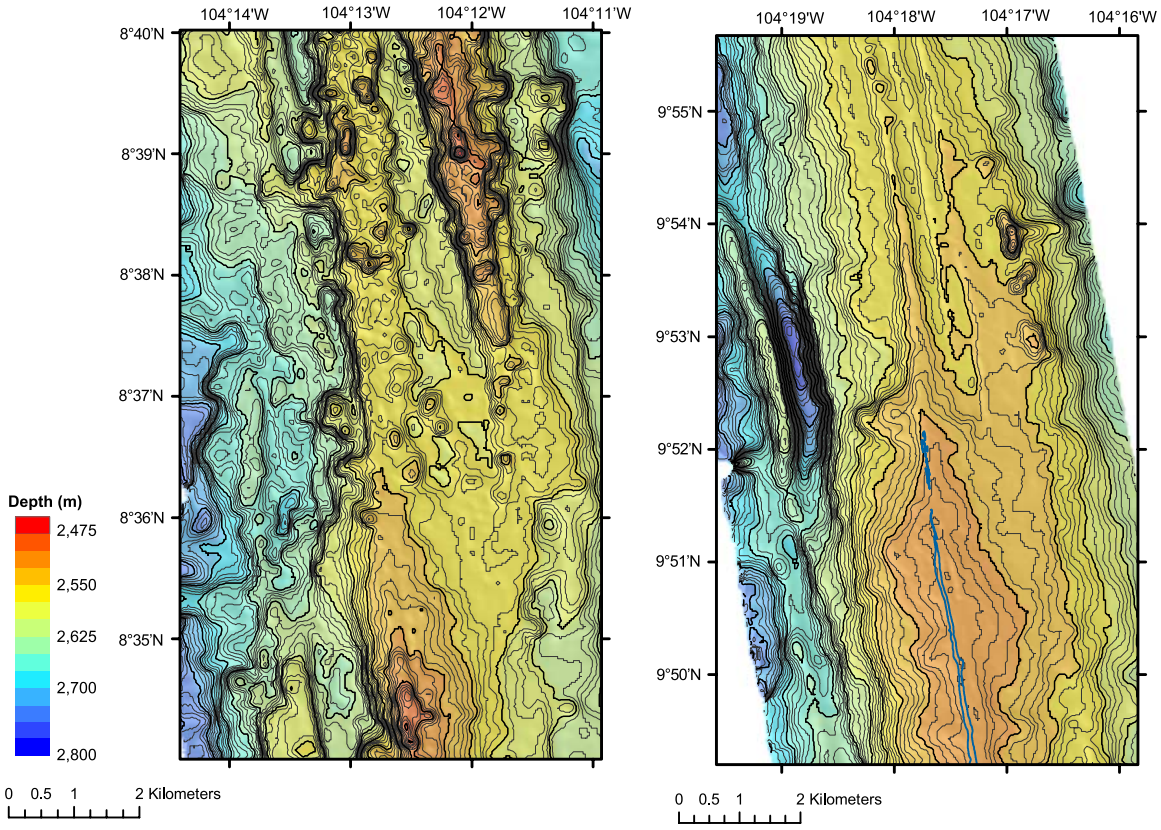

Figure 3. EM300 bathymetry of (left) third-order and (right) fourth-order ridge discontinuities. Contour interval is 5 m with a bold index contour at 25 m intervals. The third-order offset, at 8°37′N, separates an unusual segment with twin ridges to the north from a more typical segment to the south. The fourth-order discontinuity at 9°52′N is a very small right-stepping offset. Table 1 contains descriptions of these and all other ridge discontinuities in the survey area.

3-dimensional perspective provided by the EM300 data permit a refinement of the previous segment boundary picks in this area (Figure 2).

[10] Table 1 presents a comprehensive list of axial discontinuities within the Ridge 2000 Integrated Study Site, including revisions to segmentation order and adjustments to locations of segment boundary offsets based on EM300 data presented here, and high-resolution side-scan data presented previously [*Haymon et al.*, 1991; *White et al.*, 2002]. Third-order offsets typically are subtle features in the 12 kHz multibeam records, but are much more obvious from EM300 (Figure 3a). Thus our picks in Table 1 for third-order ridge discontinuities are unlikely to be changed by further mapping. Fourth-order offsets, however, usually are invisible on 12 kHz multibeam maps, and sometimes are subtle on the EM300 maps (Figure 3b). Hence future surveys with higher-resolution, well-navigated side-scan sonars are likely to better define the location and structure of fourth-order ridge discontinuities outside the 9°–10°N segment where such data already exists [*Fornari et al.*, 2004; *Haymon et al.*, 1991; *White et al.*, 2002].

4. Development of Very-Near-Axis Volcanic Cones

[11] Existing SeaBeam and SeaMARC II data from the EPR show volcanoes abruptly appearing on the ridge flanks at ~5 km from the axis, having already achieved the median volume for the entire ridge flank volcano data set [*Alexander and Macdonald*, 1996; *White et al.*, 1998]. However, only volcanoes >40 meters high can be reliably identified in these maps. Evidence exists from near-bottom observations for small-scale volcanism <2 km off-axis [*Perfit et al.*, 1994; *Schouten et al.*, 2003]. We also know that small volcanic mounds form on the crest of the ridge near ridge discontinuities [*White et al.*, 2000, 2002]. This raises the question, how far off-axis do seamounts begin to form?

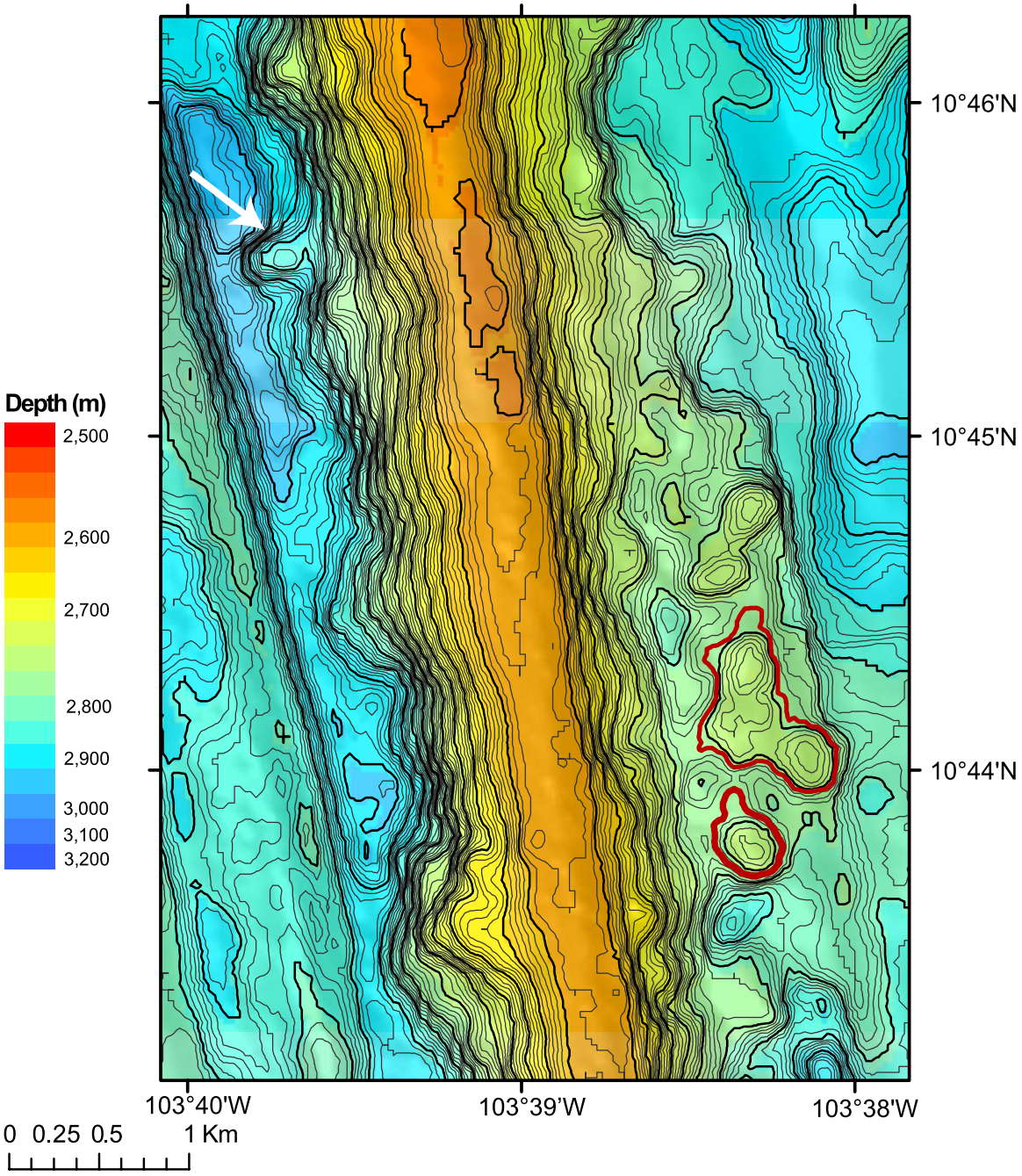

Figure 4. EM300 bathymetry showing an example of two very-near-axis cones detected by this study (bold red outlines) and a cone perched on the side of the axial high (white arrow) that was not counted in this study. The closed-contour structure to the north of the outlined volcanoes fails to meet the criteria for volcanic cone because its ratio of length:width is >2. This is also the area of the 2003 eruption of the EPR [*McClain et al.*, 2004]. Contour interval is 5 m with bold index contours at 25 m intervals.

[12] The EM300 data sets a new threshold for the detection of seamounts since we can productively contour the data at 5 m instead of 10 m as used in previous studies. Thus we can now identify volcanoes as small as ~25 m high (Figure 4). Volcanic cones were picked manually from digital maps contoured at 5 m depth intervals. All local highs defined by at least 5 contours were digitized from these maps. Only local highs with an aspect ratio of <2:1 length to width were retained as volcanic

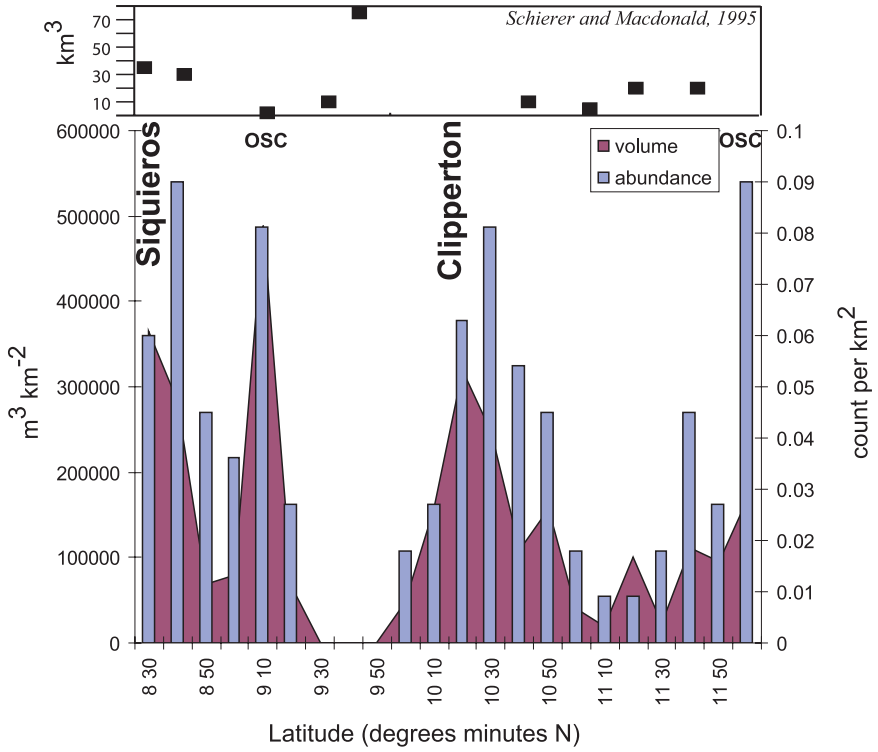

Figure 5. Comparison of the very-near-axis volcanism with the seamount chains farther off-axis. The top panel shows the volume of large off-axis seamount chains in ridge-perpendicular corridors extending from the axis to 1 Ma crust [*Scheirer and Macdonald*, 1995]. The bottom panel shows the abundance (columns) and volume (area under the curve) of very-near-axis volcanoes cataloged in this study. Local increases in both abundance and volume of very-near-axis volcanoes occur near major ridge axis discontinuities as labeled on the graph, whereas the seamounts show the opposite trend.

edifices in order to reduce the possibility of misidentifying upthrown fault blocks as volcanic cones. Several features that appear to be volcanic cones were excluded from this tabulation because the bathymetric contours do not close around the edifice. Most of the excluded features are small cones perched on the side of the axial high (Figure 4). Volcanoes were picked up to and including the Clipperton ridge-transform intersection, but were not picked within the transform. A digital elevation model created from the EM300 grids was used to calculate the height and volume of each digitized cone in our data set.

[13] Unlike the isolated off-axis volcanoes farther from the ridge axis or beyond the first set of abyssal hills, some of the cones identified in this study may be rootless cones or hornitos. These are features that grow when lava flow inflation or collapse of a lava tube cause a cone to form far from the primary eruptive vent. Features of similar size have been interpreted as rootless cones on the MAR [*Smith and Cann*, 1999]. Unfortunately, distinguishing primary vents from rootless cones formed by lava flows pouring off of the ridge axis requires on- or near-bottom geologic mapping.

[14] A total of 86 very-near-axis volcanic cones were found within the study area (Figure 2). The maximum height for all cones in the area is 110 m, the mean height is 39 ± 15 m, and the median height is 35 m. Only 12 cones are >50 m high, large enough to have been counted on the older SeaBeam maps. Of these 12 cones, three are at ~8°25′N, and the rest are between 10°N and 11°N. Approximately 30% (25 cones) lie within 1 km of the axis, thus within the axial neovolcanic zone. With only a ~6 km wide swath, there is no particular significance to the across-axis distribution. To examine the along-axis distribution of these cones we summed the total number and total volume of cones in 10′ (18.5 km) latitude bins. These data were normalized for the total area of the EM300 swath within each bin.

[15] An interesting pattern emerges in the along-axis distribution of very-near-axis cones compared to major ridge offsets (Figure 5). The cones increase in number and total volume near the major

ridge discontinuities at the Siquieros and Clipperton transforms, and at the 9°03′N and 11°45′N overlapping spreading centers (OSCs). These small cones are much more common north of Clipperton where the ridge is very narrow and erupts lower Mg basalts [*Langmuir et al.*, 1986]. This relationship contrasts with prior regional observations that seamounts are larger and more abundant where the ridge is shallowest and broadest [*Scheirer and Macdonald*, 1995] (Figure 5). Possibly these small, very-near-axis cones reflect a change in volcanic style at the ridge axis from eruption of predominately lobate lava flows to pillow lava mounds near the ends of segments [*White et al.*, 2000, 2002]. The greater abundance of pillow mounds where the ridge cross-section is narrower suggests that eruptions are both producing more mounds on-axis and burying fewer as they are rafted off-axis. We speculate that the population of volcanoes within 3 km of the axis is an expression of ridge segmentation, and part of the early growth of off-axis seamount chains.

5. Conclusions

[16] Bathymetric maps of the entire EPR ridge crest within the Ridge 2000 Program Integrated Study Site across a 6 km wide swath are presented from EM300 multibeam data collected in November 2005 (see auxiliary material[1] Animation S1). These maps are derived from data gridded at 30 m latitude by 50 m longitude, which was determined to be the finest grid interval supported by the data. This represents a greater than 4X improvement in gridcell resolution over previously available data over the ridge crest.

[17] The new EM300 bathymetry may be utilized in many different ways, to study the structure of the ridge axis or to serve as a geographic base for studies in other disciplines. Two new data products derived from the EM300 bathymetry and presented here are a revised list of ridge discontinuities within the EPR Integrated Study Site (Table 1) and the identification of 86 new volcanic cones, found near ridge discontinuities, within 3 km of the ridge axis.

Acknowledgments

[18] We thank Bill Martin, Mike Realander, and Rob Hagg of the UW marine technician group and Phil Smith of the R/V *Thompson* for assistance in collecting this data. This work benefited from discussions with Dan Fornari and Vicki Ferrini about the EM300 and Ken Macdonald about the ridge segmentation. Margo Edwards, Rob Sohn, and Doug Wilson provided insightful reviews that significantly improved the manuscript. Data collection was supported by NSF grants OCE-0326148 and OCE-0324668 and NOAA award NA04OAR4600049.

[1]Auxiliary materials are available in the HTML. doi:10.1029/2006GC001407.

References

Alexander, R. T., and K. C. Macdonald (1996), Small off-axis volcanoes on the East Pacific Rise, *Earth Planet. Sci. Lett.*, *139*, 387–394.

Berger, J., J. Orcutt, and S. Foley (2006), HiSeasNet: Oceanographic ships join the grid, *Eos Trans. AGU*, *87*, 174–175.

Carbotte, S., and K. C. Macdonald (1992), East Pacific Rise 8°–10°30′N: Evolution of ridge segments and discontinuities from SeaMARC II and three-dimensional magnetic studies, *J. Geophys. Res.*, *97*, 6959–6982.

Caress, D. W., and D. N. Chayes (1996), Improved processing of Hydrosweep DS multibeam data on the R/V Maurice Ewing, *Mar. Geophys. Res.*, *18*, 631–650.

Cochran, J. R., D. J. Fornari, B. J. Coakley, R. Herr, and M. A. Tivey (1999), Continuous near-bottom gravity measurements made with a BGM-3 gravimeter in DSV *Alvin* on the East Pacific Rise crest near 9°31′N and 9°50′N, *J. Geophys. Res.*, *104*(B5), 10,841–10,862.

Detrick, R. S., P. Buhl, E. Vera, J. Mutter, J. Orcutt, J. Madsen, and T. Brocher (1987), Multi-channel seismic imaging of a crustal magma chamber along the East Pacific Rise, *Nature*, *326*, 35–41.

Ferrini, V. L., D. J. Fornari, T. M. Shank, J. C. Kinsey, M. A. Tivey, S. A. Soule, S. M. Carbotte, L. L. Whitcomb, D. Yoerger, and J. Howland (2007), Submeter bathymetric mapping of volcanic and hydrothermal features on the East Pacific Rise crest at 9°50′N, *Geochem. Geophys. Geosyst.*, doi:10.1029/2006GC001333, in press.

Fornari, D. J., D. G. Gallo, M. H. Edwards, J. A. Madsen, M. R. Perfit, and A. N. Shor (1989), Structure and topography of the Siqueiros transform fault system: Evidence for the development of intra-transform spreading centers, *Mar. Geophys. Res.*, *11*, 263–299.

Fornari, D. J., et al. (2004), Submarine lava flow emplacement at the East Pacific Rise 9°50′N: Implications for uppermost ocean crust stratigraphy and hydrothermal fluid circulation, in *Mid-Ocean Ridges: Hydrothermal Interactions Between the Lithosphere and Oceans*, *Geophys. Monogr. Ser.*, vol. 148, edited by C. R. German, J. Lin, and L. M. Parson, pp. 187–217, AGU, Washington, D. C.

Gallo, D. G., P. J. Fox, and K. C. Macdonald (1986), A Sea Beam investigation of the Clipperton Transform Fault: The morphotectonic expression of a fast slipping transform boundary, *J. Geophys. Res.*, *91*, 3455–3467.

Haymon, R. M., D. J. Fornari, M. H. Edwards, S. Carbotte, D. Wright, and K. C. Macdonald (1991), Hydrothermal vent distribution along the East Pacific Rise Crest (9°09′–54′N) and its relationship to magmatic and tectonic processes on fast-spreading mid-ocean ridges, *Earth Planet. Sci. Lett.*, *104*, 513–534.

Kastens, K. A., W. B. F. Ryan, and P. J. Fox (1986), Structural and volcanic expression of a fast slipping ridge-transform-ridge-plate boundary: Sea MARC I and photographic surveys of the Clipperton Transform Fault, *J. Geophys. Res.*, *91*, 3469–3488.

Kent, G. M., et al. (2000), Evidence from three-dimensional seismic reflectivity images for enhanced melt supply beneath mid-ocean ridge discontinuities, *Nature*, *406*, 614–618.

Langmuir, C. H., J. F. Bender, and R. Batiza (1986), Petrological and tectonic segmentation of the East Pacific Rise, 5°30′N–14°30′N, *Nature*, *322*, 422–429.

Lee, S.-M., S. C. Solomon, and M. A. Tivey (1996), Fine-scale crustal magnetization anomalies and segmentation of the East Pacific Rise, 9°10′–9°50′N, *J. Geophys. Res.*, *101*, 22,033–22,050.

Macdonald, K. C., J.-C. Sempere, and P. J. Fox (1984), East Pacific Rise from Siqueiros to Orozco Fracture Zones: Along-strike continuity of axial neovolcanic zone and structure and evolution of overlapping spreading centers, *J. Geophys. Res.*, *89*, 6049–6069.

Macdonald, K. C., D. S. Scheirer, and S. M. Carbotte (1991), Mid-ocean ridges: Discontinuities, segments and giant cracks, *Science*, *253*, 986–994.

Macdonald, K. C., P. J. Fox, S. Carbotte, M. Eisen, S. Miller, L. Perram, D. Scheirer, S. Tighe, and C. Weiland (1992), The East Pacific Rise and its flanks, 8°–18°N: History of segmentation, propagation and spreading direction based on SeaMARC II and Sea Beam studies, *Mar. Geophys. Res.*, *14*, 299–344.

McClain, J. S., R. A. Zierenberg, J. R. Voight, K. L. Von Damm, and K. H. Rubin (2004), A recent volcanic eruption on a "magma starved" segment of the East Pacific Rise ISS, 10°44′N, *Eos Trans. AGU*, *85*(47), Fall Meet. Suppl., Abstract B13A-0177.

Perfit, M. R., D. J. Fornari, M. C. Smith, J. F. Bender, C. H. Langmuir, and R. M. Haymon (1994), Small-scale spatial and temporal variations in mid-ocean ridge crest magmatic processes, *Geology*, *22*, 375–379.

Perram, L. J., and K. C. Macdonald (1990), A one-million-year history of the 11°45′N East Pacific Rise discontinuity, *J. Geophys. Res.*, *95*, 21,363–21,381.

Scheirer, D. S., and K. C. Macdonald (1995), Near-axis seamounts on the flanks of the East Pacific Rise, 8°N to 17°N, *J. Geophys. Res.*, *100*, 2239–2259.

Schouten, H., M. Tivey, D. Fornari, D. Yoerger, A. Bradley, M. Edwards, and P. Johnson (2003), Central anomaly magnetization high: Constraints on the volcanic construction and architecture of young upper oceanic crust, EPR 9–10°N, *Ridge 2000 Events.*, *1*, 30–34.

Sempere, J.-C., and K. C. Macdonald (1986), Deep-tow studies of the overlapping spreading centers at 9°03′N on the East Pacific Rise, *Tectonics*, *5*, 881–900.

Smith, D. K., and J. R. Cann (1999), Constructing the upper crust of the Mid-Atlantic Ridge: A reinterpretation based on the Puna Ridge, Kilauea Volcano, *J. Geophys. Res.*, *104*, 25,379–25,400.

Smith, M. C., M. R. Perfit, D. J. Fornari, W. I. Ridley, M. H. Edwards, G. J. Kurras, and K. L. Von Damm (2001), Magmatic processes and segmentation at a fast spreading mid-ocean ridge: Detailed investigation of an axial discontinuity on the East Pacific Rise crest at 9°37′N, *Geochem. Geophys. Geosyst.*, *2*(10), doi:10.1029/2000GC000134.

Tighe, S. A., R. S. Detrick, P. J. Fox, C. H. Langmuir, J. C. Mutter, W. B. Ryan, and R. C. Tyce (1988), *East Pacific Rise Data Synthesis Final Report*, Joint Oceanogr. Inst. Inc., Washington, D. C.

White, S. M., K. C. Macdonald, D. S. Scheirer, and M.-H. Cormier (1998), Distribution of isolated volcanoes on the flanks of the East Pacific Rise, 15.3°–20°S, *J. Geophys. Res.*, *103*, 30,371–30,384.

White, S. M., K. C. Macdonald, and R. M. Haymon (2000), Basaltic lava domes, lava lakes, and volcanic segmentation of the southern East Pacific Rise, *J. Geophys. Res.*, *105*, 23,519–23,536.

White, S. M., R. M. Haymon, D. J. Fornari, M. R. Perfit, and K. C. Macdonald (2002), Correlation between volcanic and tectonic segmentation of fast-spreading ridges: Evidence from volcanic structures and lava flow morphology on the East Pacific Rise at 9°–10°N, *J. Geophys. Res.*, *107*(B8), 2173, doi:10.1029/2001JB000571.

Wilcock, W. S. D., D. R. Toomey, G. M. Purdy, and S. C. Solomon (1993), The renavigation of Sea Beam bathymetric data between 9°N and 10°N on the East Pacific Rise, *Mar. Geophys. Res.*, *15*, 1–12.